*remote sensing*

MDPI

*Article*

# Optimizing the Land Use and Land Cover Pattern to Increase Its Contribution to Carbon Neutrality

**Kai Wang [1], Xiaobing Li [1,*], Xin Lyu [1,2], Dongliang Dang [1], Huashun Dou [1], Mengyuan Li [1], Siyu Liu [1] and Wanyu Cao [1]**

[1] State Key Laboratory of Earth Surface Processes and Resource Ecology, Faculty of Geographical Science, Beijing Normal University, Beijing 100875, China
[2] College of Life Sciences, Beijing Normal University, Beijing 100875, China
* Correspondence: xbli@bnu.edu.cn; Tel.: +86-010-58807944

**Abstract:** Land use and land cover (LULC) contribute to both carbon storage and carbon emissions. Therefore, regulating the LULC is an important means of achieving carbon neutrality under global environmental change. Here, the West Liaohe River Basin, a semiarid watershed, was taken as a case study. Based on the assessment of the carbon storage and emissions induced by LULC from 2000–2020, we set up three different coupled shared socioeconomic pathway (SSP) and representative concentration pathway (RCP) scenarios (SSP119, SSP245, and SSP585), from 2030–2060, to optimize the LULC. Then, the LULC patterns under each scenario were simulated using the patch-generating land use simulation (PLUS) model, and the corresponding changes in carbon storage and emissions were compared and analyzed. It was found that, since 2000, with the expansion of forest, cropland, and construction land, as well as the degradation of grassland, the carbon storage and emissions induced by LULC have significantly increased, but the increase in storage was lower than that of emissions. The scenario simulations revealed that, when we optimize the LULC, mainly including the protection and expansion of ecological land such as forest and grassland in the western and southern edges of the basin, as well as the control and management of cropland land and construction land in the northeast and central parts of the basin, there will be a significant increase in the carbon storage and a significant reduction in carbon emissions from 2030–2060. This indicates that zone-based management measures with rational LULC regulation can contribute to the achievement of carbon neutrality in the study area. Supported by the results of this study, a direct decision-making basis for land use policy regulation to promote regional sustainable development can be undertaken in the basin. This study also provides a reference for low-carbon development in other regions.

**Keywords:** LULC; carbon neutrality; SSPs-RCPs; sustainable management; semiarid watershed

check for updates

**Citation:** Wang, K.; Li, X.; Lyu, X.; Dang, D.; Dou, H.; Li, M.; Liu, S.; Cao, W. Optimizing the Land Use and Land Cover Pattern to Increase Its Contribution to Carbon Neutrality. *Remote Sens.* **2022**, *14*, 4751. https://doi.org/10.3390/rs14194751

Academic Editors: Sheng Wang, Suxia Liu, Yongqiang Zhou and Raphaél Payet-Burin

Received: 23 August 2022
Accepted: 17 September 2022
Published: 23 September 2022

**Publisher's Note:** MDPI stays neutral with regard to jurisdictional claims in published maps and institutional affiliations.

**Copyright:** © 2022 by the authors. Licensee MDPI, Basel, Switzerland. This article is an open access article distributed under the terms and conditions of the Creative Commons Attribution (CC BY) license (https://creativecommons.org/licenses/by/4.0/).

## 1. Introduction

Limiting the increase in the global mean temperatures relies on reducing carbon dioxide ($CO_2$) emissions and increasing terrestrial carbon sinks [1]. As an important carbon pool in the carbon cycle, terrestrial ecosystems play an important role in addressing global climate change and achieving regional carbon neutrality. Land use and land cover (LULC) changes are some of the most significant ways that humans alter surface ecosystems [2], and LULC can affect the carbon storage of terrestrial ecosystems through exerting complex impacts on the structures, patterns, processes, and functions of ecosystems [3]. In addition, LULC is also a major carrier of carbon emissions [4]. Carbon emissions due to global LULC changes in 2020 reached 0.9 ± 0.7 Gt of C [5], which has become the second largest source of carbon emissions after fossil fuel combustion [6]. Therefore, a scientific and rational approach to LULC management is essential for the realization of the carbon neutrality goal under the background of global environmental change.

To achieve the carbon neutrality goal, countries around the world have implemented many initiatives [7], among which the optimization of LULC is an important way at the

fundamental level and an important part of nature-based solutions [8]. It is important to analyze the LULC changes related to carbon storage and carbon emissions variation, which can timely identify the problems in the process of LULC development in the past and provide an important reference for LULC management. In recent years, research on the impact of LULC changes on the carbon cycle in terrestrial ecosystems has become a hot topic [9–11]. For example, Chang et al. explored the effects of LULC changes on terrestrial carbon storage in China from 2000 to 2018, and they found that large carbon losses have occurred as a result of deforestation, whereas carbon gains have occurred as a result of the activity, cultivation, and afforestation related to the Grain to Green Project [6]. Zhang et al. took the Yellow River Delta as a study area, analyzed the spatial and temporal distribution characteristics of carbon emissions, caused by land use changes from 2000 to 2019, and found that the total net carbon emissions increased rapidly, which was mainly due to the expansion of construction land as a carbon source [12]. Overall, previous studies have mostly analyzed the impact of LULC changes on the terrestrial carbon cycle in terms of either carbon storage or carbon emissions, but it is necessary to estimate both the carbon storage and carbon emissions induced by LULC, which can provide us with a better understanding of the relative changes between them and lay a solid foundation for optimal land use regulation, facilitating the achievement of the carbon neutrality goal. Besides, the objective of climate change mitigation is to stabilize and reduce the concentrations of greenhouse gases in the atmosphere and, as a corollary, to maximize carbon storage in terrestrial ecosystems, which also requires comprehensive carbon accounting [13].

With the advancement of land use research, the effects of future land use changes on the terrestrial carbon cycle have emerged as a new research field [14–16]. Future scenarios enable the establishment of an effective connection between future land use simulations and optimal land use regulation by describing different future development possibilities, which has attracted a number of scholars to conduct related studies [17,18]. When simulating future land use changes, the drivers of land use change have been confirmed to have an important impact on the uncertainty of the simulation results. However, most studies tend to default to the drivers of land use change by maintaining the drivers in the historical period, ignoring the future climate and socioeconomic variability across scenarios and the impact of their long-term temporal changes on the LULC [19], which may affect the realism of the resulting land use simulations and the formulation of countermeasures and proposals for practical land use management. The latest Coupled Model Intercomparison Project Phase 6 (CMIP6) model has been proven to provide researchers with multiple reasonable future global climate and socioeconomic change scenarios by coupling shared socioeconomic pathways (SSPs) and representative concentration pathways (RCPs) [20,21]. The RCPs define a set of climate-forcing pathways, while the SSPs outline five alternative socioeconomic development scenarios. Therefore, it is important to couple the possible future climate and socio-economic conditions in the SSP–RCP scenarios, when simulating land use patterns in the process of setting up different scenarios, to further improve the feasibility of land use optimization.

The West Liaohe River Basin is located in the upper reaches of the Liaohe River Basin, which is one of the seven major basins in China. As a typical semiarid watershed containing mountains, water, forests, fields, lakes, grasslands, and sand, it plays an important role in regional carbon neutrality. This basin has been the main implementation area of many ecological restoration projects in China since the end of the last century, and as the most important economic development area in eastern China, urbanization has been accelerating, resulting in significant changes in the regional LULC, which have affected the carbon storage and emissions. Therefore, the purpose of this study was to optimize the LULC pattern in the West Liaohe River Basin in order to increase its contribution to carbon neutrality. First, the spatiotemporal variations in carbon storage and emissions, from 2000 to 2020, were analyzed based on the integrated valuation of ecosystem services and tradeoffs (InVEST) model and the carbon emission model, respectively [22,23]. Furthermore, based on the carbon neutrality–future land use simulation–optimal land use regulation

process, we set up three different scenarios (SSP119, SSP245, and SSP585) that couple the possible future climate and socio-economic conditions of the SSPs and RCPs. Based on a comparative analysis of the LULC simulation results and the carbon storage and emissions changes under each scenario, we put forward a series of practical land use optimization and regulation measures for the West Liaohe River Basin. The results of this study provide directional guidance for the optimal management of current and future LULC in the study area, thus better contributing to the achievement of the carbon neutrality goal.

## 2. Materials and Methods

### *2.1. Study Area*

The West Liaohe River Basin (116°36′–123°40′E, 41°18′–45°13′N), located in the eastern part of the three northern junction areas of the farming–pastoral ecotone in northern China, is an important ecological barrier and an important base of the energy and coal chemical industries in northern China [24]. The basin is fan-shaped, and the river mainly flows through the two prefecture-level cities of Chifeng and Tongliao in Inner Mongolia, with an administrative scope that includes 21 counties (banners) and a total watershed area of about 12.65 × $10^4$ $km^2$. The terrain is high in the west and low in the east, ranging from 15 to 2052 m. It has the typical vegetation characteristics of the transition zone between the semi-humid and semi-arid areas. Located in the temperate zone of East Asia, it has a continental monsoon climate with distinct seasons. The main climatic characteristics are aridity and low rainfall, and the annual average temperature gradually increases from northwest to southeast by 5–6.5 °C. The annual precipitation is 350–550 mm [25]. Grassland and cropland occupy more than 70% of the basin, and the northern and southern edges of the watershed are dominated by forests. In addition, the Horqin Sandy Land, the largest sandy land in China, is located in the study area (Figure 1).

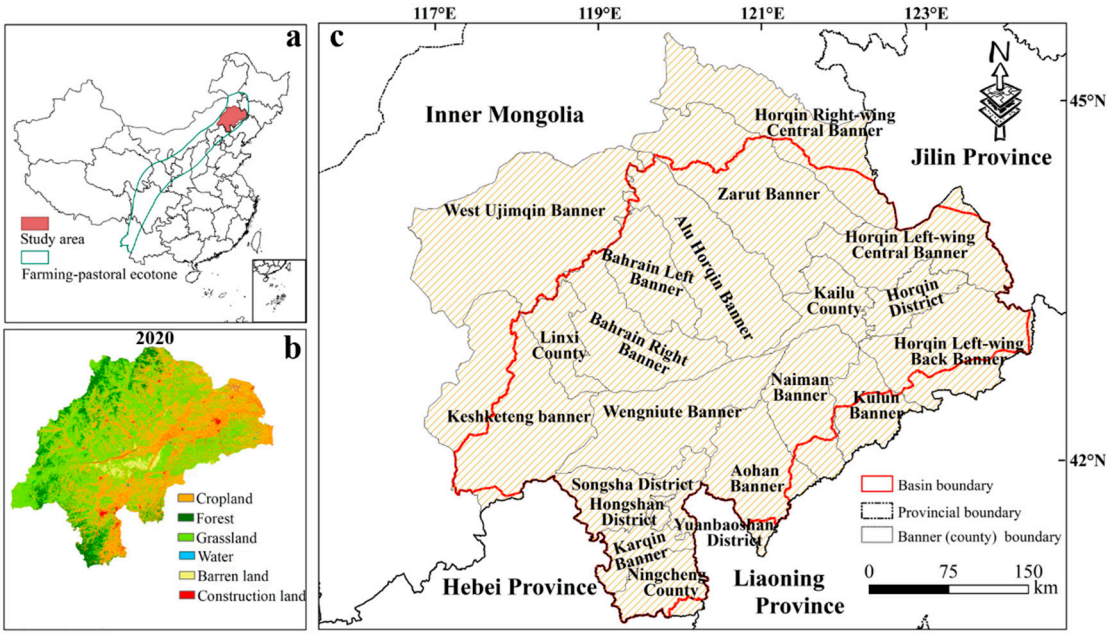



**Figure 1.** Location of the study area. (**a**) The farming–pastoral ecotone in China; (**b**) the distribution of land use in 2020; (**c**) the 21 counties (banners) covered by the study area.

With the accelerated urbanization and agriculturalization, frequent agricultural reclamation, overgrazing, and other human activities in the Western Liaoning River Basin have caused environmental problems, such as the continuous expansion of the arable land, degradation of the grasslands, and shrinkage of the wetlands [26], which have had negative effects on the vegetation and soil carbon pool. Therefore, there is an urgent need to optimize the LULC management in the Western Liaohe River Basin, according to the

carbon source/sink characteristics of each land use type, in order to help reach the carbon neutrality goal.

### *2.2. Data Sources and Preprocessing*

The basic data used in this study included a time-series LULC dataset, which is an important input for evaluating carbon storage and carbon emissions induced by LULC and for simulating future scenarios. In this study, we used the first Landsat-derived 30 m annual China land cover dataset (CLCD) from 2000 to 2020 [27]. It consists of nine classes: cropland, forest, shrubland, grassland, water, snow and ice, barren land, impervious surfaces, and wetland. Based on the actual situation of the study area and the land use classification of this dataset, the land use/cover types were reclassified into six classes: cropland, forest, grassland, water, barren land, and construction land. In addition, the drivers of LULC changes are important data inputs for conducting land use simulations, which mainly included natural factors, accessibility, and socioeconomic factors in this study. The specific data presentation and sources are presented in Table 1. The other socioeconomic panel data (including energy data and regional gross domestic product (GDP)) were obtained from the China Energy Statistical Yearbook and the corresponding city statistical yearbooks (2001–2021).

To simulate the LULC changes under different future scenarios, we selected four major drivers (i.e., GDP, population, temperature, and precipitation) that change significantly in future scenarios and have a strong influence on the LULC changes [28]. The gridded GDP and population data were obtained from the datasets for the different SSPs (SSP1, SSP2, and SSP5) provided by Murakami et al. [29] and Chen et al. [30], respectively. The temperature and precipitation data for scenarios SSP119, SSP245, and SSP585 were obtained from the National Earth System Science Data Center (http://www.geodata.cn/, accessed on 22 May 2022); which have been downscaled to 1 × 1 km resolution using the Delta spatial downscaling scheme in China.

**Table 1.** Specific description of each driver and its source.

| Specific Data | Type | Resolution | Source |
|---|---|---|---|
| 1 km monthly temperature dataset for China (2000–2020) | Raster | 1 km | National Earth System Science Data Center (http://www.geodata.cn/, accessed on 27 December 2021) |
| 1 km monthly precipitation dataset for China (2000–2020) | Raster | 1 km | |
| ASTER DEMv3 | Raster | 30 m | |
| Slope | Raster | 30 m | Calculated using the slope module in ArcGIS 10.2 based on the DEM. |
| Aspect | Raster | 30 m | |
| Road distribution | Shapefile (polyline) | N/A | National Catalogue Service for Geographic Information (https://www.webmap.cn/commres.do?method=result100, accessed on 5 September 2022) |
| River distribution | Shapefile (polyline) | N/A | |
| Settlement distribution | Shapefile (points) | N/A | |
| GDP density | Raster | 1 km | Resource and Environment Science and Data Centre of the Chinese Academy of Sciences (https://www.resdc.cn/, accessed on 25 April 2022) |
| Population density | Raster | 1 km | |

Note: The 1 km monthly temperature and precipitation dataset for China was spatially downscaled from the 30′ Climatic Research Unit (CRU) time series dataset with the climatology dataset of WorldClim using delta spatial downscaling by Peng et al. [31], which has been updated to 2020. Based on this dataset, we derived the average precipitation and average temperature for 2000–2020 to conduct our study. The accessibility factors included the distance to roads (railway and roads), the distance to the river, and the distance to settlements, which were calculated using the Euclidean distance tool in ArcGIS 10.2.

### *2.3. Research Methods*

#### 2.3.1. Research Framework

The research framework of this paper is shown in Figure 2. Firstly, based on the long-time series LULC dataset from CLCD, the spatiotemporal variations in carbon storage and emissions, from 2000 to 2020, were systematically analyzed based on the InVEST model

and the carbon emission model, respectively. Secondly, the LULC changes under scenarios SSP119, SSP245, and SSP585, from 2030 to 2060, were simulated using the PLUS model [14]. Then, the corresponding changes in the carbon storage and emissions were predicted. Finally, based on comparative analysis of the LULC simulation results and the carbon storage and emission changes under each scenario, a series of practical LULC optimization and regulation measures for the study area were designed.

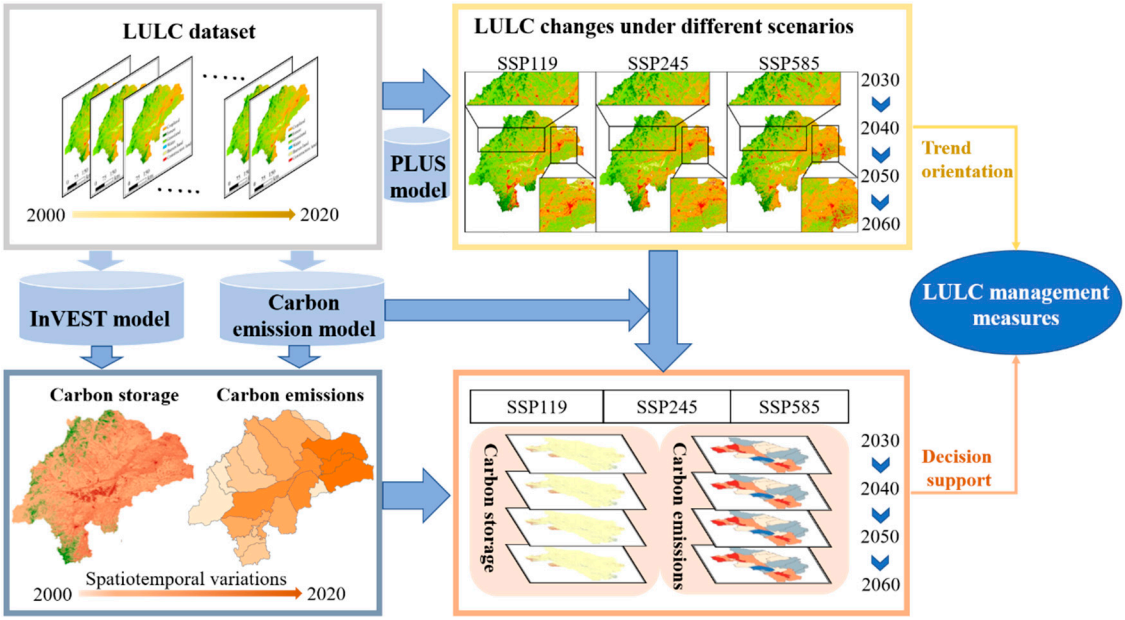



**Figure 2.** The research framework of this paper.

2.3.2. Calculation of Carbon Storage Induced by LULC

In this study, the carbon storage and sequestration module in the InVEST model was used to evaluate the changes in carbon storage, in the study area, from 2000 to 2020. This module simplifies the ecosystem carbon cycle process by mainly combining the LULC data to calculate the carbon storage of the ecosystem. It divides the ecosystem carbon storage into four basic carbon pools: aboveground carbon storage; belowground carbon storage; soil organic carbon storage; dead organic matter carbon storage [22,32]. The specific calculation formula is shown in Equation (1):

$$C_t = \sum_{j=1}^{n=6} A_j \left( C_{aj} + C_{bj} + C_{cj} + C_{dj} \right) \quad (1)$$

where $C_t$ is the total carbon storage (t); j denotes the land use type; n is the total number of land use types (six in this study); $A_j$ is the area of land use type j (ha); $C_{aj}$ is the above-ground carbon density of land use type j (t/ha); $C_{bj}$ is the below-ground carbon density of land use type j (t/ha); $C_{cj}$ is the soil carbon density of land use type j (t/ha) at a certain depth (0–30 cm in this study); $C_{dj}$ is the carbon density of the dead organic matter of land use type j (t/ha). The specific carbon density of each land use type is presented in Table S1 in the Supplementary Files [33–36].

2.3.3. Calculation of Carbon Emissions Induced by LULC

Carbon emissions induced by LULC consist of two parts: direct carbon emissions and indirect carbon emissions [12]. In this study, the direct carbon emissions were defined as the carbon emissions from five land use types—cropland, forest, grassland, water, and barren land—mainly from agricultural machinery energy consumption, fertilizer application,

domestic sewage, biological respiration, and soil organic matter decomposition [23]. The specific calculation formula is as follows:

$$E_k = \sum_{i=1}^{n=6} A_i \times \delta_i, \quad (2)$$

where $E_k$ is the direct carbon emissions (kg); $i$ denotes the land use type; n is the total number of land use types (six in this study); $A_i$ is the area of land use type $i$ ($m^2$); $\delta_i$ is the carbon emissions (absorption) coefficient for land use type $i$. Referring to existing studies, the $\delta_i$ values for the land use types are presented in Table 2.

**Table 2.** Carbon emissions coefficients of each land use type and their sources.

| Land Use Types | Mean Carbon Emission Coefficient ($kg/m^2$) | Source |
|---|---|---|
| Cropland | 0.0422 | [37] |
| Forest | −0.0644 | [37,38] |
| Grassland | −0.0021 | [37,38] |
| Water | −0.0253 | [12,23] |
| Barren land | −0.0005 | [37] |

Indirect carbon emissions, which are caused by construction sites, consist primarily of emissions from fossil fuel combustion and industrial processes. The emissions from the latter source are much smaller (accounting for 9.89% of the total emissions) than that from fossil fuel combustion [39], so this fraction was not considered in this study. The carbon emissions from fossil energy combustion were calculated using the Intergovernmental Panel on Climate Change (IPCC) model and fossil energy consumption data. The specific calculation formula is as follows:

$$E_m = \sum E_{nj} \times \sigma_j \times \gamma_j, \quad (3)$$

where $E_m$ is the indirect carbon emissions (kg); $E_{nj}$ is the consumption of fossil energy $j$ (kg); $\sigma_j$ is the conversion factor from fossil energy source $j$ to standard coal ($kgce \cdot kg^{-1}$); $\gamma_j$ is the carbon emission factor of energy source $j$ ($t \cdot t^{-1}$). The main types of energy needed for production and living include raw coal, coke, crude oil, gasoline, kerosene, diesel oil, fuel oil, natural gas, and electric power. In this study, the conversion factors of the various fossil energy sources to standard coal and the corresponding carbon emissions factors were obtained from the China Energy Statistics Yearbook and the IPCC Guidelines for National Greenhouse Gas Emission Inventories, respectively. These values are presented in Table S2 in the Supplementary Files.

It should be noted that energy consumption data were obtained from energy balance tables (EBTs), but the relevant statistical yearbooks in China only provide EBTs on the national or provincial scale [40]. The China Energy Statistical Yearbook is only updated until 2020. Therefore, based on the EBTs for Inner Mongolia, the indirect carbon emissions in the study area, from 2000 to 2019, were obtained based on the ratio of the sum of the GDPs of Chifeng and Tongliao to the GDP of Inner Mongolia by referring to a related study [12]. In addition, in order to visualize the spatial distribution characteristics of the carbon emissions in the study area, the total indirect emissions were divided by the total area of the construction land in the 21 counties (banners) covered by the study area to obtain the average carbon emissions of the construction land [41]. Then, we analyzed these data at the county scale by combining the carbon emissions coefficients of the other land use types.

#### 2.3.4. Simulation of LULC Pattern Based on the Patch-Generating Land UseSimulation (PLUS) Model

The PLUS model was developed based on the cellular automata (CA) model, a tool for patch-scale LULC change simulation based on raster data. It mainly consists of two

parts: a land expansion analysis strategy (LEAS) based on the random forest (RF) algorithm and a CA model based on multi-type random patch seeds (CARS) [42]. The software for the PLUS is available at https://github.com/HPSCIL/Patch-generating_Land_Use_Simulation_Model (accessed on 25 April 2022).

In the LEAS module, a land expansion map, obtained based on the two periods of LULC data and multiple driving factors, is required. It uses the RF model to explore the relationships between the growths of each land use type in order to obtain the development probability of each land use type. Based on the LEAS results, and after obtaining the quantitative demand for each land use type under each scenario based on Markov chains, the CARS module simulates the patch evolution of the multiple land use types using a multi-type random patch seeding mechanism based on threshold descent [42].

To evaluate the simulation performance of the PLUS model used in this study, both the overall accuracy (OA) and Cohen's kappa coefficient (Kappa) were used to evaluate the modeling accuracy. The formula for calculating Kappa is as follows:

$$\text{Kappa} = (P_0 - P_c)/(P_p - P_c), \quad (4)$$

where $P_0$ is the proportion of actual simulations that are correct, $P_c$ is the proportion of simulations that are correct in the random case, and $P_p$ is the proportion of simulations that are correct in the ideal case. Kappa ranges from 0 to 1. In general, when Kappa < 0.4, the simulation results are considered to be in poor agreement with the actual situation, with large variations [43].

#### 2.3.5. Establishment of Multiple Coupled SSP–RCP Scenarios

In the latest CMIP6 phase, the combination of RCPs and SSPs makes future scenarios more reasonable. Based on retaining the four typical representative concentration pathways of CMIP5, it adds three new pathways and emphasizes the consistency of each RCP scenario and SSP scenario, thus forming eight combined scenarios [44]. Based on the new combinations of RCPs and SSPs, we set up three different scenarios that couple three representative concentration pathways (RCP1.9, RCP4.5, and RCP 8.5) and three alternative policy scenarios (SSP1, SSP2, and SSP5) to simulate the future land-use patterns from 2030 to 2060 [28].

1. SSP1-RCP1.9 (SSP119)

SSP119 (integrated scenario of SSP1 and RCP1.9 of CMIP6) is a sustainable scenario that focuses on ecological restoration and conservation, and it significantly reduces the dependence on fossil fuels [21]. This means that the LULC regulation should not only focus on ecological lands such as forest and grassland but also on construction land, which is the main place where fossil fuels are combusted [45]. Therefore, in this study, based on the Markov chains and the land use transfer matrix from 2010 to 2020, the probability of the conversion of other land use types to forest and grassland is higher, while the probability of conversion to built-up land is reasonably limited from 2030 to 2060.

2. SSP2-RCP4.5 (SSP245)

SSP245 (integrated scenario of SSP2 and RCP4.5 of CMIP6) describes a natural development scenario that emphasizes the development of socioeconomic and climatic conditions while maintaining the pattern of change over the past decades [28,44]. This means that LULC regulation only needs to be carried out in accordance with the past LULC changes. Therefore, in this study, the land use changes from 2030 to 2060 are consistent with the transfer probability from 2010 to 2020, with more conversion of grassland to other land use types and more conversion of other land use types to construction land.

3. SSP5-RCP 8.5 (SSP585)

SSP585 (integrated scenario of SSP5 and RCP8.5 of CMIP6) is a scenario of rapid economic development at the cost of the heavy use of fossil fuels, with a significant increase in socioeconomic conditions but substantial greenhouse gas emissions [28,44]. This means

that the LULC regulation tends to focus on changes in construction land that are closely related to economic growth [46]. Therefore, in this study, based on the Markov chains and the land use transfer matrix from 2010 to 2020, the probability of the creation of construction land and the conversion of forest and grassland to other land use types increases from 2030 to 2060.

## 3. Results

### *3.1. Spatiotemporal Variations in Carbon Storage and Emissions from 2000 to 2020*

In this study, the carbon storage in the study area from 2000 to 2020 was assessed year by year (detailed information is provided in Figure S1), and its spatial and temporal variation characteristics during this period were obtained. The results (Figure 3a) show that the spatial distribution of the carbon storage in the study area was generally high in the west and low in the east, but some areas were too high or too low, with higher carbon storage mainly occurring in the forest land at the edge of the basin and lower carbon storage occurring in the sandy land in the central part of the study area. The change trend of the average carbon storage during this period (Figure 3b) suggests that the mean carbon storage in the study area significantly increased (slope = 0.829, $p < 0.001$) from 140.98 t in 2000 to 148.44 t in 2020. Furthermore, we also analyzed the changes in the carbon storage of the different carbon pools from 2000 to 2020 (Figure 3b). It was found that the increase in the total carbon storage in the study area was mainly controlled by the increase in the aboveground carbon storage (slope = 0.987, $p < 0.001$). The soil organic carbon storage was the main contributor to the total carbon storage (more than 50%), but there was no significant change during this period (slope = 0.145, $p > 0.05$).

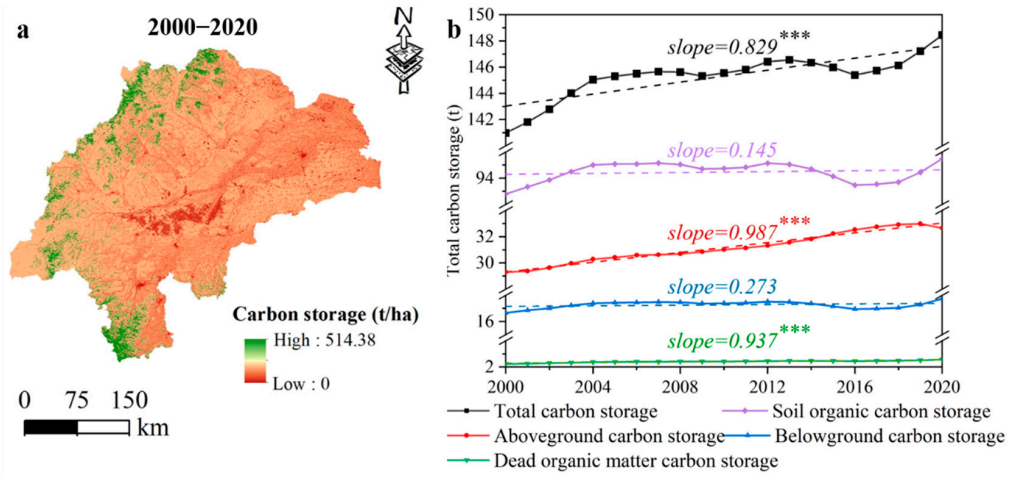



**Figure 3.** Spatiotemporal changes in carbon storage in the study area from 2000 to 2020. (**a**) The spatial distribution of the average carbon storage; (**b**) the changes in the carbon storages of the different carbon pools. Note: *** denotes significance at the 0.001 level.

Figure 4 shows the temporal and spatial variation characteristics of the carbon emissions in the study area during the past 20 years. The results (Figure 4a) show that the spatial distribution of the carbon emissions in the study area was generally high in the east and low in the west. Moreover, the areas with high carbon emissions were mainly distributed in the counties dominated by cultivated land, while the areas with low carbon emissions were mainly distributed in the counties dominated by forest land and grassland. The change trend of the average carbon emissions during this period (Figure 4b) suggests that the total carbon emissions in the study area significantly increased (slope = 0.814, $p < 0.001$) from 464.95 $\times$ $10^4$ t in 2000 to 1986.86 $\times$ $10^4$ t in 2020. Compared with the direct carbon emissions, the indirect carbon emissions from the construction land were the main contributors to the total carbon emissions, accounting for more than 70% (Figure 4b). Moreover, the significant increase in the carbon emissions from the construction land signif-

icantly contributed to the increase in the total carbon emissions in the study area (Figure 4c) (slope = 0.814, $p < 0.001$). Figure 4c shows the changes in the carbon emissions from the other land use types from 2000 to 2019. It can be seen that cropland, as another major carbon emissions source in addition to construction land, did not change significantly during the past 20 years (slope = 0.288, $p > 0.05$). As the major contributors to carbon uptake, the grassland, water, and barren land underwent different degrees of decline (slope = 0.496, $p < 0.05$; slope = 0.875, $p < 0.001$; slope = 0.530, $p < 0.05$, respectively), while the forest land increased significantly (slope = −0.993, $p < 0.001$).

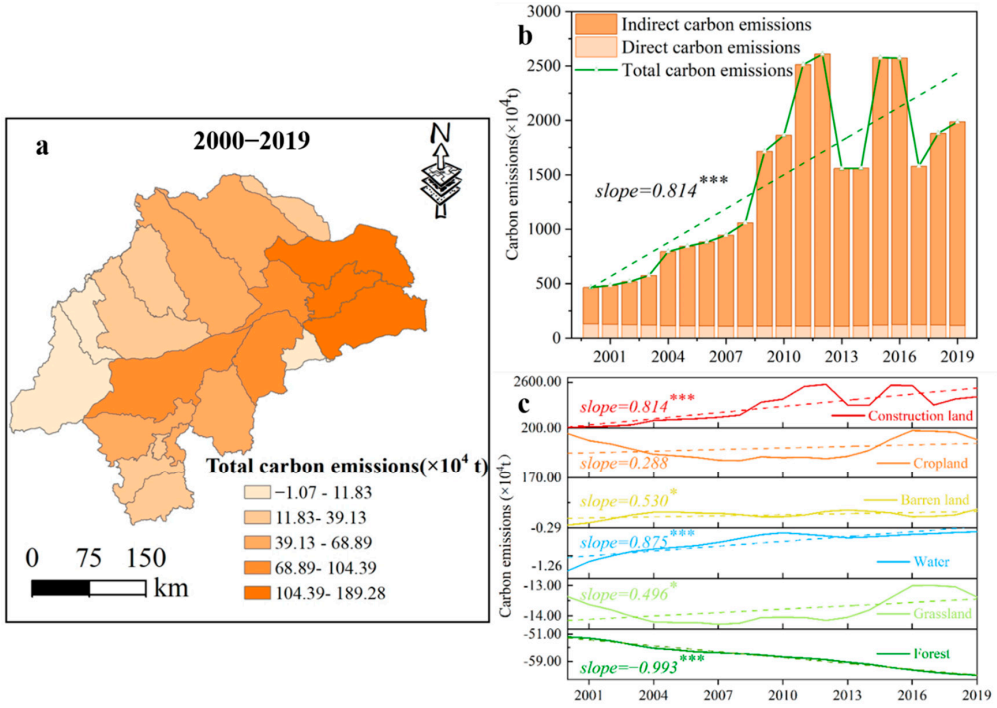



**Figure 4.** Changes in carbon emissions in the study area from 2000 to 2019. (**a**) The spatial distribution of the multi-year average carbon emissions; (**b**) the changes in the total carbon emissions; (**c**) the changes in the carbon emissions from the different land use types. Note: * denotes significance at the 0.05 level, and *** denotes significance at the 0.001 level.

### *3.2. Comparison of Spatiotemporal Changes in LULC under SSP–RCP Scenarios*

In this study, in order to verify the applicability of the PLUS model to the study area, we simulated the 2020 LULC based on the 2010 LULC data using the PLUS model. Then, the results were compared with and validated against the actual LULC in 2020. The simulation performance evaluation revealed that the OA was 0.85, and the kappa coefficient was 0.74. These results indicate that the PLUS model established a reliable dynamic simulation and can be reliably used to predict future land use in the study area.

Figure 5 shows the simulated land use patterns under the different scenarios, and Figure 6 shows the changes in the areas of the different land use types in the historical period and under the future scenarios. The results show that the grassland and cropland will still occupy the majority of the land use structure in the study area, but the spatial distribution and change in the area of each land use type exhibit significant differences under the different SSP–RCP scenarios. Overall, from 2030 to 2060, under scenario SSP119, the cropland will shrink, the forest and grassland will expand, and the construction land will increase, but the rates of these changes are the lowest among the three scenarios. Under scenario SSP245, the cropland and grassland will decrease, while the forest and construction land will increase. The rates of change of the land use types under this scenario are between those of scenarios SSP119 and SSP585. Under scenario SSP585, the cropland, forests, and construction land will all increase, while the grassland will shrink significantly (Figure 6).

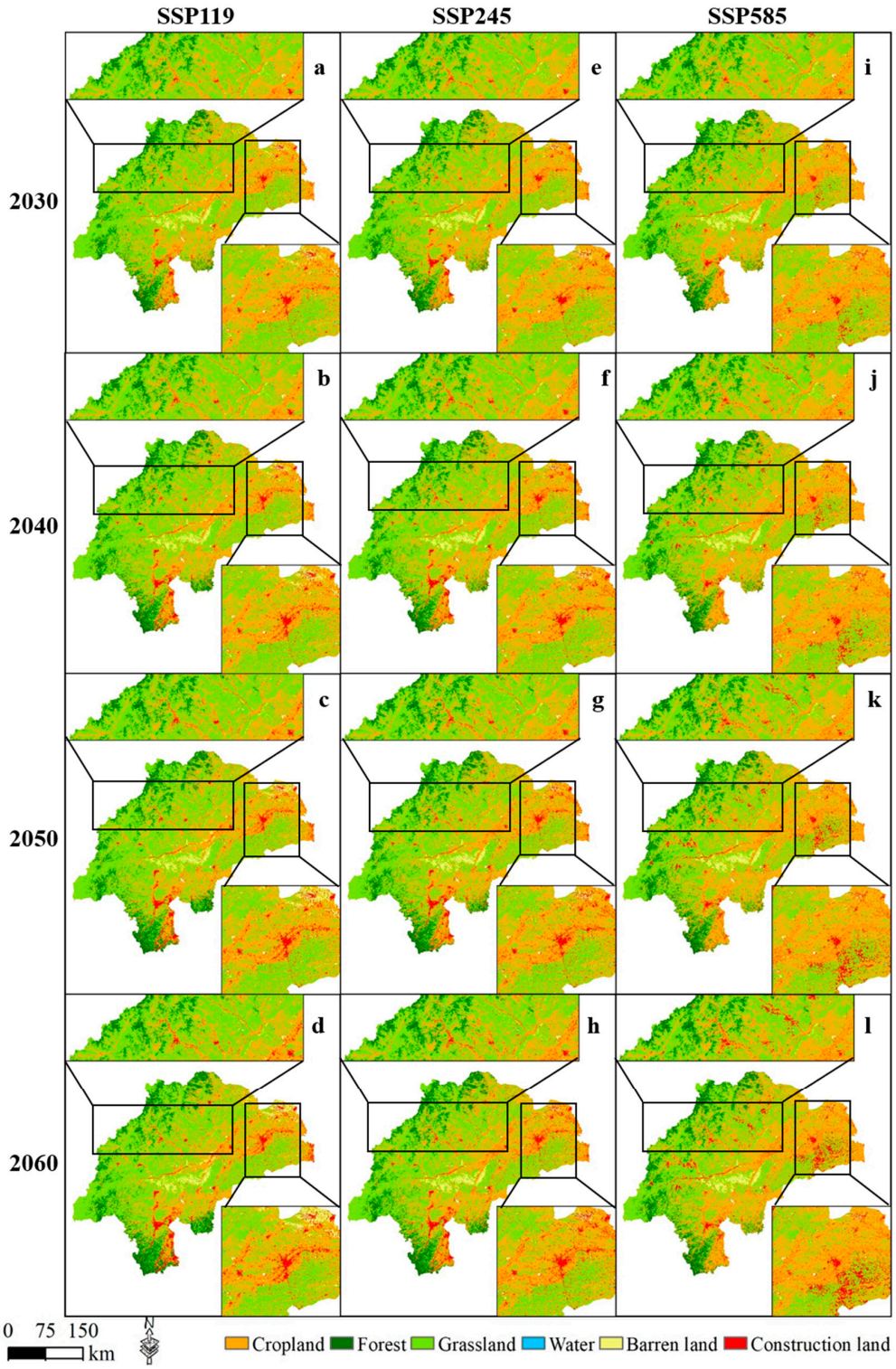



**Figure 5.** LULC patterns under SSP119 (**a**–**d**), SSP245 (**e**–**h**), and SSP585 (**i**–**l**) for four future periods: 2030s, 2040s, 2050s, and 2060s.

Specifically, under scenario SSP119, the cropland will decrease the most compared to the changes under the other two scenarios, decreasing by 14.5% from 2030 to 2060 (Figure 6a). In contrast, the increase in the construction land will be the smallest among the three scenarios (Figure 6f). In addition, both the forests and grasslands will significantly increase from 2030 to 2060, increasing by 18.7% and 1.7%, respectively, which are higher than under the other two scenarios (Figure 6b,c). It can be seen that the expansion of

the forest land will mainly occur in the southern part of the study area in the Aohan Banner (Figure 5a–d). Under scenario SSP245, the spatial variations and area changes of the cropland, forests, and construction land, from 2030 to 2060, are similar to those under scenario SSP119, but the rates of change in their areas are significantly different (Figures 5a–h and 6a,b,f). Although the grassland remains the land use type with the greatest proportion in the study area, from 2030 to 2060, it will undergo a slow increase (2020–2040), followed by a sudden decrease (2040–2060) (Figure 6c), resulting in an overall decrease in the area of grassland. Under scenario SSP585, in contrast to the other two scenarios, the cropland will significantly increase by 4.5% from 2030 to 2060, and this increase will mainly occur in the northeastern part of the basin (Figures 5i–l and 6a), while the grassland will significantly decrease by 7.0% from 2030 to 2060 (Figure 6c). The forest land will increase, but its area in 2060 will be much smaller than under the other two scenarios (Figure 6b). The construction land will expand the most under all three scenarios, mainly in local areas in the northeastern and northwestern regions of the basin. This differs from the other two scenarios in which the construction land expands in the southern part of the basin (Figures 5 and 6f).

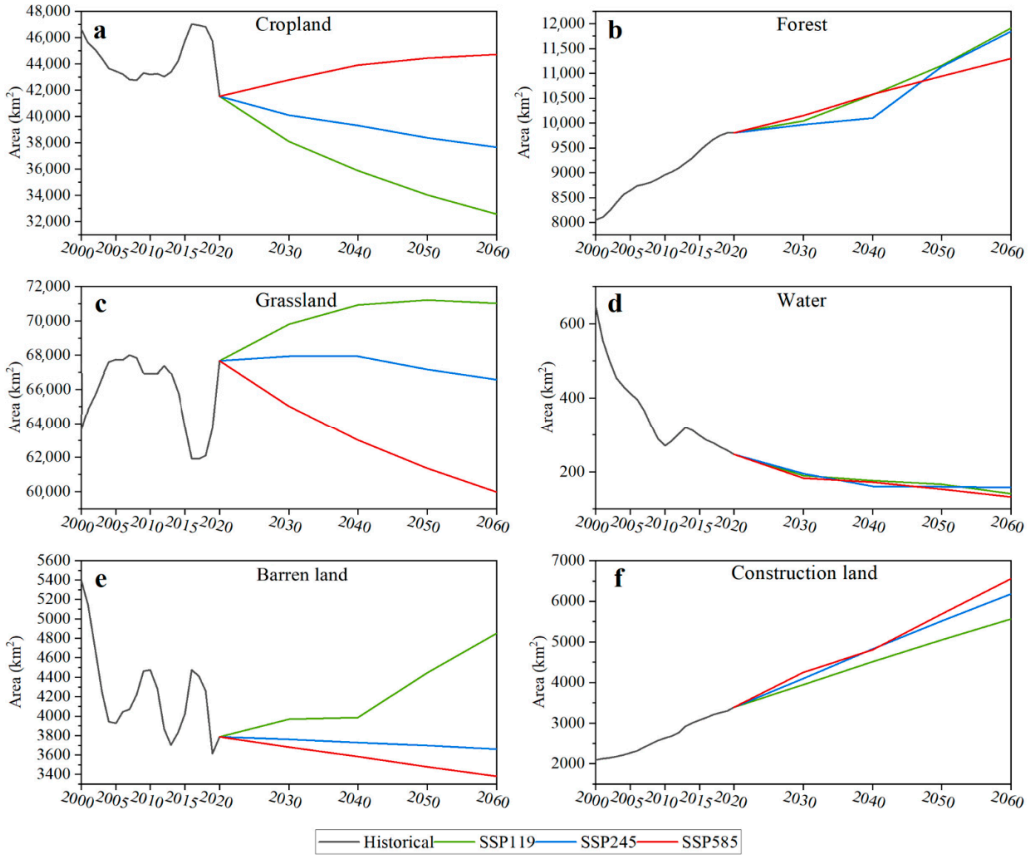



**Figure 6.** Area statistics of cropland (**a**), forest (**b**), grassland (**c**), water (**d**), barren land (**e**) and construction land (**f**) during the historical period and under the future scenarios.

### *3.3. Estimation of Carbon Storage and Emissions under SSP–RCP Scenarios*

Based on the results of the future land use simulations, the changes in the carbon storage, compared to 2020, under the different SSP–RCP scenarios, at different times in the study area, were assessed (Table 3; Figure 7). The results (Table 3) show that there will be an increase in the carbon storage from 2030 to 2060 under scenarios SSP119 and SSP245, but there will be no significant change under scenario SSP585. However, the increasing trends differ under scenarios SSP119 and SSP245. Under scenario SSP119, the mean carbon storage will increase from 149.62 t in 2030 to 154.49 t in 2060, maintaining a growth rate of 0.8%

to 1.1% per decade. Under scenario SSP245, although the mean carbon storage exhibits an overall increasing trend from 148.73 t in 2030 to 152.94 t in 2060, there will be a slight decrease during the first 20 years. Figure 8 shows the changes in the spatial distribution of the carbon storage under each scenario compared to 2020. It can be seen that the proportion of the regions with increasing carbon storage trends is higher than that of the regions with decreasing carbon storage trends under scenarios SSP119 and 245, from 2030 to 2060, but the opposite occurs under scenario SSP585.

**Table 3.** Carbon storage under the future scenarios at different times.

| Carbon Storage (t) | Multiple Coupled SSP–RCP Scenarios | | |
|---|---|---|---|
| | SSP119 | SSP245 | SSP585 |
| 2020 | 148.44 | 148.44 | 148.44 |
| 2030 | 149.62 | 148.73 | 148.25 |
| 2040 | 151.33 | 148.64 | 148.61 |
| 2050 | 152.68 | 151.29 | 148.64 |
| 2060 | 154.49 | 152.94 | 148.72 |

Specifically, the areas in which the carbon storage increases under scenarios SSP119 and SSP245 are located on the northern and southern edges of the study area, which is consistent with the areas in which the forest expansion occurs. The increase in the area of grassland will also contribute to the increase in carbon storage under scenario SSP119. In addition, it should be noted that there will be a slight decrease in carbon storage on the northeastern edge of the study area, from 2030 to 2060, under scenario SSP119, which will be accompanied by the conversion of cropland to unused land in this area. Unlike the other two scenarios, under scenario SSP585, there will be a significant decline in local areas in the northeastern and northwestern regions of the basin where the built-up land will undergo sharp expansion. However, at the same time, the areas on the western edge of the basin will exhibit a slight increase, which may lead to a lack of a significant change in carbon storage from 2030 to 2060 (Figure 7).

Similarly, we predicted the changes in the carbon emissions compared to 2019 under the different scenarios based on the results of the future LULC simulations (Table 4; Figure 8). It should be noted that, in the absence of future energy consumption data, in order to facilitate the prediction of the future carbon emissions, the average value of the construction land-averaged carbon emissions, from 2000 to 2019, was taken as the carbon emissions coefficient of the construction land [41]. The results (Table 4) revealed that, although there will be an increase in carbon emissions from 2030 to 2060 under all of the scenarios, under scenario SSP119, the growth rate of the carbon emissions is consistently much lower than under the other two scenarios during the same period, except for the similar rate of change from 2030 to 2040 under scenario SSP585. As shown in Figure 8, these regions will gradually expand, which will increase the carbon emissions under all of the scenarios, but there are some variations in the locations at which this will occur.

**Table 4.** Carbon emissions under future scenarios at different times.

| Carbon Emissions ($\times 10^4$ t) | Multiple Coupled SSP–RCP Scenarios | | |
|---|---|---|---|
| | SSP119 | SSP245 | SSP585 |
| 2019 | 1986.86 | 1986.86 | 1986.86 |
| 2030 | 1709.31 | 1780.67 | 1854.59 |
| 2040 | 1930.36 | 2075.39 | 2084.77 |
| 2050 | 2137.19 | 2347.43 | 2446.82 |
| 2060 | 2337.32 | 2616.78 | 2805.97 |

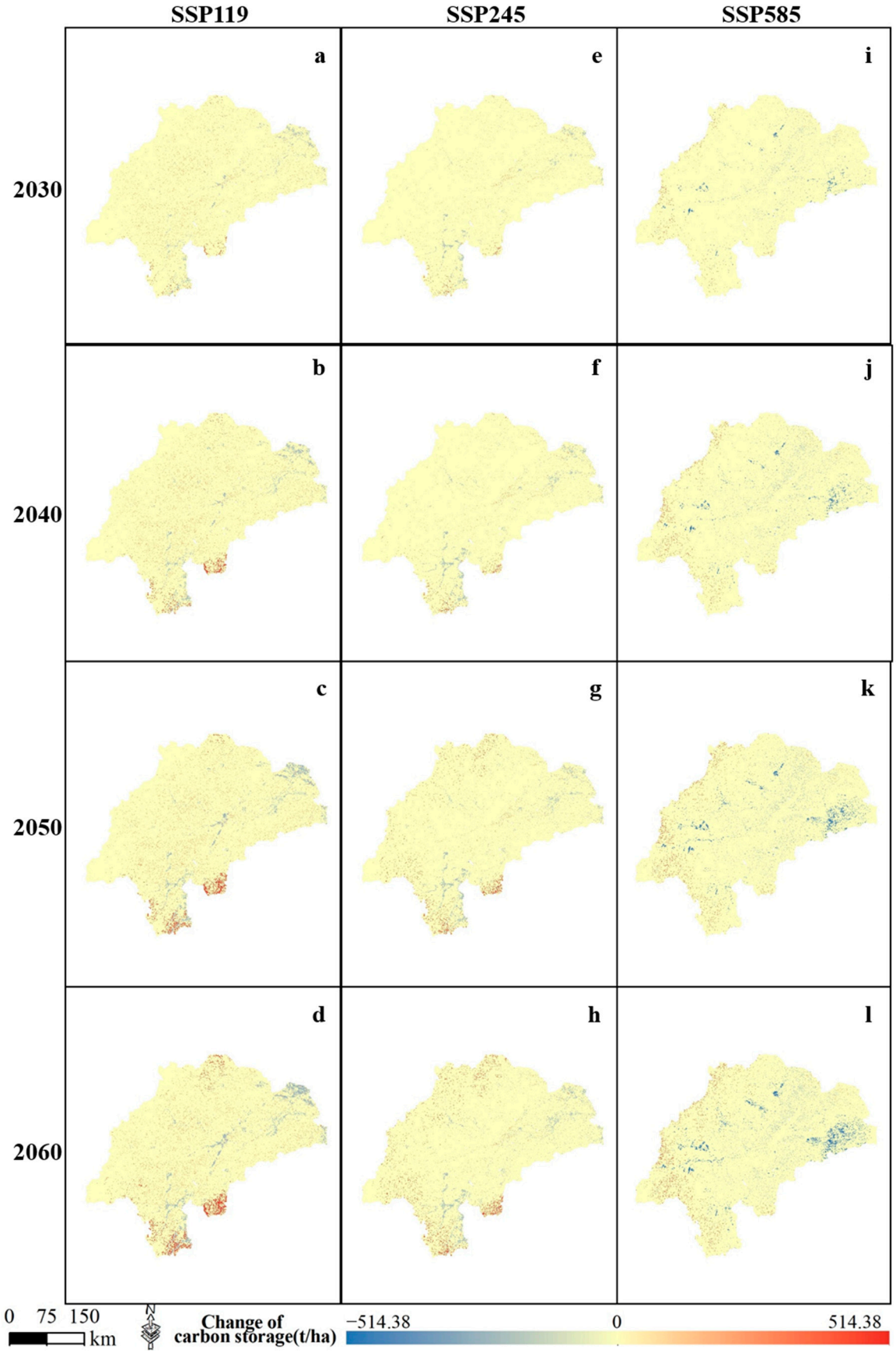



**Figure 7.** Changes in the spatial distribution of the carbon storage compared to 2020 under SSP119 (**a**–**d**), SSP245 (**e**–**h**), and SSP585 (**i**–**l**) for four future periods: 2030s, 2040s, 2050s, and 2060s.

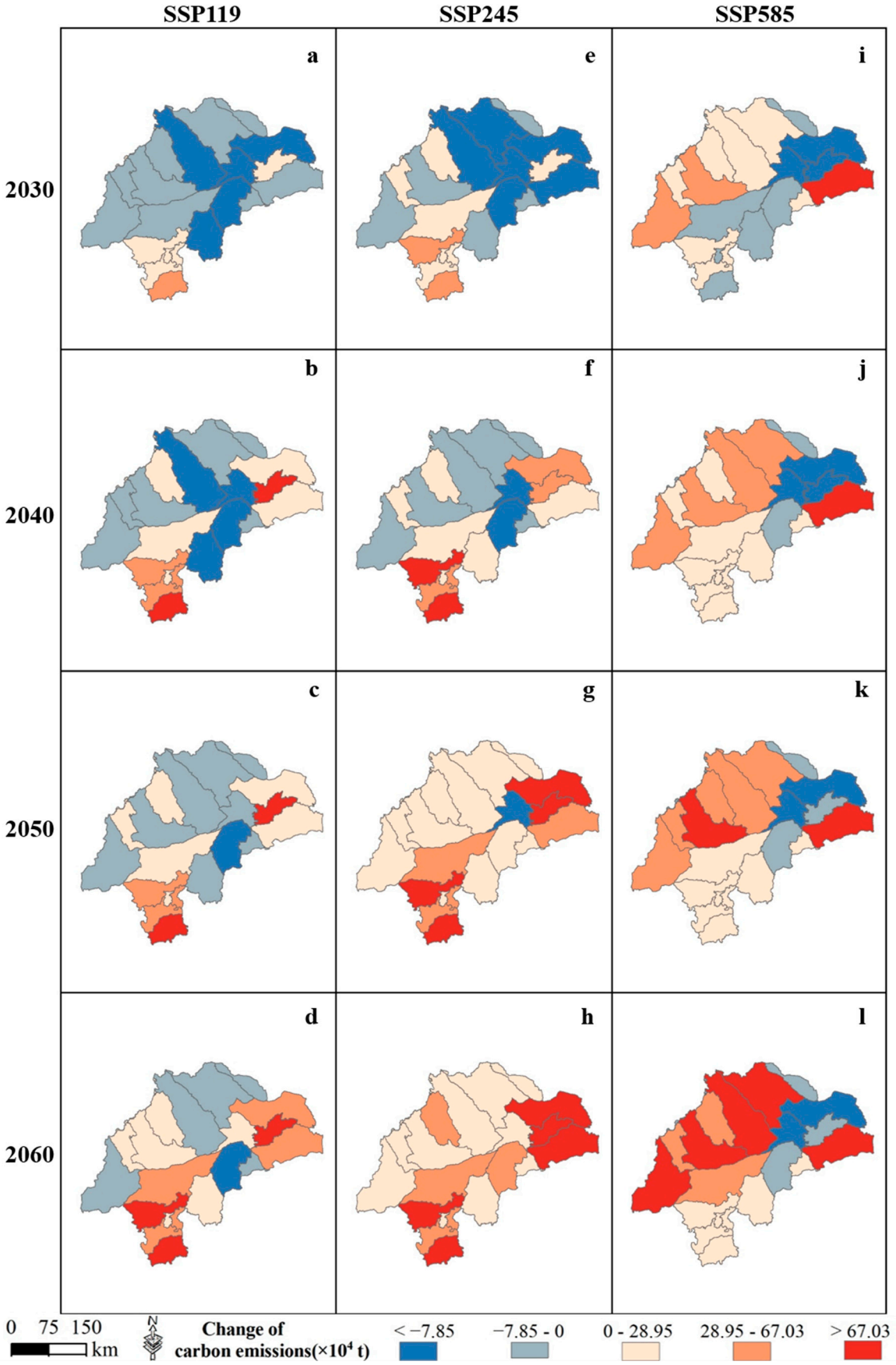



**Figure 8.** Changes in the spatial distribution of the carbon emissions compared to 2019 under SSP119 (**a**–**d**), SSP245 (**e**–**h**), and SSP585 (**i**–**l**) for four future periods: 2030s, 2040s, 2050s, and 2060s.

Specifically, under scenario SSP119, the southern and northern parts of the basin will maintain a decreasing carbon emissions trend by 2060. This corresponds to the main locations of the forests and grassland in the study area. The areas with increasing carbon emissions trends are located in the southern and northeastern counties (banners), corresponding to the places where construction land will continue to expand. The locations of these areas are the same under scenario SSP245. In particular, there will be an increasing carbon emissions trend throughout the study area under scenario SSP245, but most of the increases will be slight to moderate compared to those under scenario SSP585. Under scenario SSP585, the western part of the basin will maintain an increasing trend, and the rate of increase will continue to increase. However, there will be a decrease in the carbon emissions in the central and eastern part of the basin under this scenario, which is consistent with the location of the significant expansion of cropland.

## 4. Discussion

### *4.1. Analysis of the Influence of LULC Changes on Carbon Storage and Emissions*

Land use and land cover changes not only directly influence carbon storage in terrestrial ecosystems but also indirectly affect anthropogenic carbon emissions [45,47]. In order to fully understand the impact of LULC on the terrestrial carbon cycle and to formulate reasonable and effective land use management measures, in this study, a more comprehensive carbon accounting analysis was carried out compared to those conducted in previous studies [17,48]. In this analysis, we not only assessed the carbon storage induced by LULC, but also estimated the carbon emissions induced by the LULC.

It was found that the characteristics changes in the carbon storage and carbon emissions, in the study area, coincided with land use changes with a high degree of consistency. As shown in Figures 3a and 4a, spatially, the carbon storage in the study area was high in the west and low in the east during the historical period, which was the opposite of the distribution pattern of the carbon emissions, and it was mainly dominated by the long-standing spatial pattern of the LULC in the study area. The western part of the basin contains most of the forest and grassland, which have great carbon sink capacities [49], while the eastern part is mainly cropland and construction land, which have low elevations and support a large population (Figure 1b). Thus, this area is more likely to have more agriculture and industrial activities, generating high levels of carbon emissions [23]. Moreover, the time series trends of the carbon storage (2000–2020) and carbon emissions (2000–2019) illustrate the specific impact of the quantitative changes in the main land use types (Figures 3b and 4b). Along with the implementation of several ecological restoration projects such as the Three North Protection Forests, the West Liaohe River Basin has established a pattern of rapid afforestation in an increasingly large area, which has significantly increased the vegetation coverage and enriched the above-ground carbon pool [50], resulting in the accumulation of carbon and an increase in the total carbon storage. However, the increase in the carbon storage was not as large as the increase in the carbon emissions caused by the rapid expansion of construction land, especially industrial land. Construction land is the main site for industry, population, buildings, transportation, and public services, making it the main carrier of carbon emissions [51]. The related human activities (material and energy consumption) also generate high carbon emissions [52]. In addition, due to natural factors and human interventions, the expansion of cultivated land and the shrinkage of grassland were almost inevitable in the agro-pastoral ecotone of northern China [53], which was also found in the results of this study. Moreover, the loss of ecosystem carbon pools, especially soil carbon storage, caused by agro-pastoral patterns, characterized by the cropland and grassland, having opposite change trends has been well documented [54,55]. All of these factors have weakened the carbon sequestration capacity of the West Liaohe River Basin to some extent and have led to increased carbon emissions.

Overall, the LULC changes in the West Liaohe River Basin, from 2000 to 2020, significantly influenced the related carbon storage and carbon emissions. The gap between the two was obvious, and there is still a great deal of room for emissions reduction. Therefore,

it is urgent that the land use and land cover pattern should be optimized by making full use of the carbon source/sink characteristics of each land use type.

### 4.2. Regional LULC Optimization Management towards Carbon Neutrality

The results of the comparative analysis of the changes in the carbon storage and carbon emissions, induced by LULC changes under the three scenarios, demonstrate that the contribution of the LULC to carbon neutrality can be increased when it is regulated in a green and sustainable way. It was found that the increase in carbon storage is significantly enhanced, while carbon emissions are significantly reduced under scenario SSP119 from 2030 to 2060 compared with those under scenarios SSP245 and SSP585 (Tables 3 and 4). In terms of the corresponding land use changes, the changes in the grassland and cropland under scenario SSP119 are distinctly different from those under the other two scenarios, that is, significant shrinkage of cropland and expansion of grassland (Figure 6). Therefore, based on the fact that cropland is a carbon source while grassland is a carbon sink, it is necessary to reasonably implement fallowing, no-tilling, and less-tilling practices, as well as to strengthen the protection and restoration of grassland in the West Liaohe River Basin to promote carbon neutrality. It should be noted that, with the advancement of urbanization and industrialization, the agricultural labor force in rural areas is increasing at an accelerating rate, and the hollowing out of towns and the aging of the rural population are intensifying [56]. Cropland may gradually develop into unused land, such as under scenario SSP119 (Figure 5a–d). In this process, the organic matter input into the soil is restricted due to the sparse vegetation cover and the high proportion of bare soil [57]. In addition, the root biomass input in croplands is lower in young and sparsely vegetated abandoned croplands [58]. This can lead to a significant decrease in carbon stocks in areas of abandoned cropland, which is not conducive to regional carbon neutrality. Therefore, in the management of cropland in the West Liaohe River Basin, attention should be paid to the prevention of the abandonment phenomenon, especially on the northeastern edge of the basin.

Although scenario SSP119 provides the main direction for land use optimization, scenarios SSP245 and SSP585 provide land management insights that should not be ignored. First, due to urbanization and continuous socio-economic development, humans need more space for activities under both scenarios [53], which is directly manifested in the expansion of construction land under all of the scenarios (Figures 5 and 6f). However, if no restrictions are imposed, as is demonstrated by scenario SSP585, a considerable amount of other land use types, especially grassland, will be transformed into built-up areas, which will result in a high level of carbon emissions, even though the increased forest area under this scenario will curb carbon emissions and increase carbon stocks in some areas. This highlights the importance of limiting the expansion of construction land with high carbon emissions intensity and improving the space-intensive utilization efficiency of the existing construction land [59]. In addition, the carbon storage in the northwestern and southern edges of the study area corresponds to the forest expansion area, exhibiting a significant increase under all three scenarios. This is mainly due to the increased carbon sink capacity of the ecosystem as a result of forest expansion [1,60]. However, it should be noted that if scenarios SSP245 and SSP585 are continued in the northwestern region until 2060, due to the continuous expansion of human activities, some of the grassland and forest land will be replaced by construction land (Figure 5e–l), which will also lead to a high level of carbon emissions (Figure 8e–l). This indicates that the western part of the basin, corresponding to the distribution areas of the forest and grassland, is an area vulnerable to human disturbance, so the promotion of key ecological projects and large-scale national greening should be strengthened based on the maintenance of the existing forest ecosystem. Besides, in order to maximize the carbon sink potential of the forest and grassland in the study area, attention should be paid to the protection of the grassland while preventing the encroachment of construction land on the forest, grassland, and other ecological lands. The results of our study emphasize the importance of increasing the

carbon storage by increasing the forest coverage, but Piao et al. have found that the carbon sink effect of afforestation will weaken as the forest ages [61]. Therefore, it is necessary to manage and nurture the existing and newly planted forests to extend the service time of their carbon sink.

In summary, the essence of the initiative, optimizing the LULC pattern to increase its contribution to carbon neutrality, is to increase the land use types with low carbon emissions intensities and limit the land use types with high carbon emissions intensities [45]. Moreover, we should not simply focus on surface expansion but should reasonably plan land use through zoning management measures to ensure that the outer ring of the ecological management area surrounds the cropland and construction land remediation areas, based on meeting local economic development needs and preserving the native characteristics of the ecosystem (Figure 9).

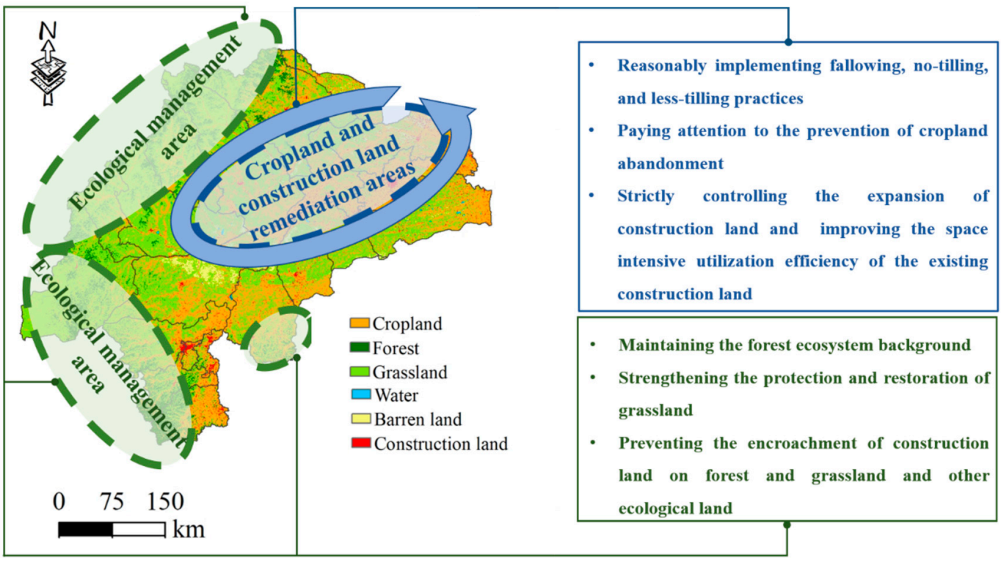



**Figure 9.** Zoning management measures for land use optimization and management in the study area.

### *4.3. Limitations and Future Directions*

In this study, the possible future land-use patterns under coupled SSP–RCP scenarios were mapped, and the corresponding carbon storage and carbon emissions were estimated, providing a solid scientific basis for coping with future climate change and socioeconomic development, as well as achieving carbon neutrality. However, this study also has some limitations that need to be addressed in future research. Primarily, the carbon storage (CS) module in the InVEST model has been widely considered to be suitable for carbon storage assessment [17,55], but the limitations of this model must be recognized, among which the most prominent limitation is the invariable carbon density setting for each land use type. Although we have localized the data based on field survey data in this study, the changes in the long-term data sequences cannot be ignored. In addition, when estimating future carbon emissions, we calculated the future indirect carbon emissions from construction land by introducing a construction land-average carbon emission coefficient [41]. Although it is a good solution to the problem that indirect carbon emissions are difficult to obtain if future energy consumption data are unknown, the use of average values makes the overall carbon emissions underestimated (Table 4). In future work, we need to open up the black box underlying this model tool and integrate more land surface ecological process models and remote sensing technology means to more scientifically and rationally assess the dynamics of the carbon storage and carbon emissions [62].

## 5. Conclusions

In this study, firstly, the spatiotemporal variations in carbon storage and emissions, induced by LULC in the West Liaohe River Basin from 2000 to 2020, were systematically analyzed, thus achieving comprehensive carbon accounting. Then, based on the PLUS model and remote sensing data sources, the LULC under scenarios SSP119, SSP245, and SSP585 from 2030 to 2060 were simulated, and the corresponding changes in the carbon storage and emissions were predicted. On this basis, regional LULC optimization management measures for promoting carbon neutrality were designed. The results of this study reveal that both the carbon storage and emissions, induced by LULC in the study area, underwent significant changes from 2000 to 2020, and there is still a great deal of room for emission reductions. To facilitate the achievement of the carbon neutrality goal, the optimal management of the LULC in the West Liaohe River Basin should be carried out through zoning management measures, under which the outer ring of the ecological management area should surround the cropland and construction land remediation areas. The results of this study can not only provide a new insight into regional LULC optimization management to achieve the carbon neutrality goal, thus supporting decision-making for implementing nature-based solutions to better respond to future climate change, but also provide a model reference for low carbon development in similar regions in different parts of the globe.

**Supplementary Materials:** The following supporting information can be downloaded at: https://www.mdpi.com/article/10.3390/rs14194751/s1, Table S1: Carbon density of each land use type in the InVEST model; Table S2: Conversion factor to standard coal from different types of energy and carbon emission coefficient; Figure S1: Spatial and temporal distribution of carbon storage in the study area from 2000 to 2020. References [33–36] are cited in the supplementary materials.

**Author Contributions:** Conceptualization, K.W., X.L. (Xiaobing Li), X.L. (Xin Lyu), D.D. and H.D.; Data curation, K.W., M.L., S.L. and W.C.; Funding acquisition, X.L. (Xiaobing Li); Methodology, K.W., X.L. (Xin Lyu) and D.D.; Project administration, X.L. (Xiaobing Li); Software, K.W.; Supervision, X.L. (Xiaobing Li); Formal analysis, K.W.; Writing (original draft preparation), K.W., X.L. (Xiaobing Li), X.L. (Xin Lyu) and D.D.; Writing (reviewing and editing), K.W., X.L. (Xiaobing Li), X.L. (Xin Lyu), D.D. and H.D.; and Visualization, K.W. All authors have read and agreed to the published version of the manuscript.

**Funding:** This research was funded by the Key Science and Technology Special Program of the Inner Mongolia Autonomous Region (grant no. 2021ZD0015-01 and 2021ZD0011-04) and the Project Supported by the State Key Laboratory of Earth Surface Processes and Resource Ecology (grant no. 2022-ZD-02).

**Data Availability Statement:** The data that support the findings of this study are available from the corresponding author upon reasonable request.

**Conflicts of Interest:** The author declares no conflict of interest.

## References

1. Wang, J.; Feng, L.; Palmer, P.I.; Liu, Y.; Fang, S.; Bösch, H.; O'Dell, C.W.; Tang, X.; Yang, D.; Liu, L.; et al. Large Chinese land carbon sink estimated from atmospheric carbon dioxide data. *Nature* **2020**, *586*, 720–723. [CrossRef]
2. Winkler, K.; Fuchs, R.; Rounsevell, M.; Herold, M. Global land use changes are four times greater than previously estimated. *Nat. Commun.* **2021**, *12*, 2501. [CrossRef]
3. Li, Z.; Xia, J.; Deng, X.; Yan, H. Multilevel modelling of impacts of human and natural factors on ecosystem services change in an oasis, Northwest China. *Resour. Conserv. Recycl.* **2021**, *169*, 105474. [CrossRef]
4. Huang, Y.; Zhang, B.; Xu, G.; Hao, W. Swelling behaviours and mechanical properties of silk fibroin–polyurethane composite hydrogels. *Compos. Sci. Technol.* **2013**, *84*, 15–22. [CrossRef]
5. Friedlingstein, P.; Jones, M.W.; O'Sullivan, M.; Andrew, R.M.; Bakker, D.C.E.; Hauck, J.; Le Quéré, C.; Peters, G.P.; Peters, W.; Pongratz, J.; et al. Global Carbon Budget 2021. *Earth Syst. Sci. Data* **2022**, *14*, 1917–2005. [CrossRef]
6. Chang, X.; Xing, Y.; Wang, J.; Yang, H.; Gong, W. Effects of land use and cover change (LUCC) on terrestrial carbon stocks in China between 2000 and 2018. *Resour. Conserv. Recycl.* **2022**, *182*, 106333. [CrossRef]
7. Mallapaty, S. How China could be carbon neutral by mid-century. *Nature* **2020**, *586*, 483. [CrossRef]

8. Seddon, N.; Daniels, E.; Davis, R.; Chausson, A.; Harris, R.; Hou-Jones, X.; Huq, S.; Kapos, V.; Mace, G.M.; Rizvi, A.R.; et al. Global recognition of the importance of nature-based solutions to the impacts of climate change. *Glob. Sustain.* **2020**, *3*, e15. [CrossRef]
9. Houghton, R.A.; Hackler, J.L. Sources and sinks of carbon from land-use change in China. *Glob. Biogeochem. Cycles* **2003**, *17*, 1034. [CrossRef]
10. Zhang, P.; He, J.; Hong, X.; Zhang, W.; Qin, C.; Pang, B.; Li, Y.; Liu, Y. Carbon sources/sinks analysis of land use changes in China based on data envelopment analysis. *J. Clean. Prod.* **2018**, *204*, 702–711. [CrossRef]
11. Zhang, F.; Xu, N.; Wang, C.; Wu, F.; Chu, X. Effects of land use and land cover change on carbon sequestration and adaptive management in Shanghai, China. *Phys. Chem. Earth Parts A/B/C* **2020**, *120*, 102948. [CrossRef]
12. Zhang, C.-Y.; Zhao, L.; Zhang, H.; Chen, M.-N.; Fang, R.-Y.; Yao, Y.; Zhang, Q.-P.; Wang, Q. Spatial-temporal characteristics of carbon emissions from land use change in Yellow River Delta region, China. *Ecol. Indic.* **2022**, *136*, 108623. [CrossRef]
13. Keith, H.; Vardon, M.; Obst, C.; Young, V.; Houghton, R.A.; Mackey, B. Evaluating nature-based solutions for climate mitigation and conservation requires comprehensive carbon accounting. *Sci. Total Environ.* **2021**, *769*, 144341. [CrossRef] [PubMed]
14. Tian, L.; Tao, Y.; Fu, W.; Li, T.; Ren, F.; Li, M. Dynamic Simulation of Land Use/Cover Change and Assessment of Forest Ecosystem Carbon Storage under Climate Change Scenarios in Guangdong Province, China. *Remote Sens.* **2022**, *14*, 2330. [CrossRef]
15. Li, J.; Chen, X.; Kurban, A.; Van de Voorde, T.; De Maeyer, P.; Zhang, C. Coupled SSPs-RCPs scenarios to project the future dynamic variations of water-soil-carbon-biodiversity services in Central Asia. *Ecol. Indic.* **2021**, *129*, 107936. [CrossRef]
16. Wang, Z.; Li, X.; Mao, Y.; Li, L.; Wang, X.; Lin, Q. Dynamic simulation of land use change and assessment of carbon storage based on climate change scenarios at the city level: A case study of Bortala, China. *Ecol. Indic.* **2022**, *134*, 108499. [CrossRef]
17. Zhu, W.; Zhang, J.; Cui, Y.; Zhu, L. Ecosystem carbon storage under different scenarios of land use change in Qihe catchment, China. *J. Geogr. Sci.* **2020**, *30*, 1507–1522. [CrossRef]
18. He, H.; Zhao, Y.; Wu, J. Simulation of urban landscape pattern under the Influence of Low Carbon: A Case Study of Shenzhen. *Acta Ecol. Sin.* **2021**, *41*, 8352–8363.
19. Fang, Z.; Ding, T.; Chen, J.; Xue, S.; Zhou, Q.; Wang, Y.; Wang, Y.; Huang, Z.; Yang, S. Impacts of land use/land cover changes on ecosystem services in ecologically fragile regions. *Sci. Total Environ.* **2022**, *831*, 154967. [CrossRef]
20. Eyring, V.; Bony, S.; Meehl, G.A.; Senior, C.A.; Stevens, B.; Stouffer, R.J.; Taylor, K.E. Overview of the Coupled Model Intercomparison Project Phase 6 (CMIP6) experimental design and organization. *Geosci. Model Dev.* **2016**, *9*, 1937–1958. [CrossRef]
21. Su, B.; Huang, J.; Mondal, S.K.; Zhai, J.; Wang, Y.; Wen, S.; Gao, M.; Lv, Y.; Jiang, S.; Jiang, T.; et al. Insight from CMIP6 SSP-RCP scenarios for future drought characteristics in China. *Atmos. Res.* **2021**, *250*, 105375. [CrossRef]
22. Sharp, R.; Chaplin-Kramer, R.; Wood, S.; Guerry, A.; Douglass, J. *InVEST User's Guide*; The Natural Capital Project, Stanford University: Stanford, CA, USA; University of Minnesota: Minneapolis, MN, USA; The Nature Conservancy: Arlington County, VA, USA; World Wildlife Fund: Morges, Switzerland, 2018.
23. Yang, B.; Chen, X.; Wang, Z.; Li, W.; Zhang, C.; Yao, X. Analyzing land use structure efficiency with carbon emissions: A case study in the Middle Reaches of the Yangtze River, China. *J. Clean. Prod.* **2020**, *274*, 123076. [CrossRef]
24. Liu, D.; Chen, J.; Ouyang, Z. Responses of landscape structure to the ecological restoration programs in the farming-pastoral ecotone of Northern China. *Sci. Total Environ.* **2020**, *710*, 136311. [CrossRef]
25. Lyu, X.; Li, X.; Wang, K.; Cao, W.; Gong, J.; Wang, H.; Lou, A. Linking regional sustainable development goals (RSDGs) with ecosystem services to identify ecological security patterns. *Land Degrad. Dev.* **2022**. [CrossRef]
26. Zhu, W.; Gao, Y.; Zhang, H.; Liu, L. Optimization of the land use pattern in Horqin Sandy Land by using the CLUMondo model and Bayesian belief network. *Sci. Total Environ.* **2020**, *739*, 139929. [CrossRef] [PubMed]
27. Yang, J.; Huang, X. *The 30 m Annual Land cover Datasets and Its Dynamics in China from 1990 to 2021*, version 1.0.1.; Zenodo; OpenAIRE: Los Angeles, CA, USA, 2022. [CrossRef]
28. Zhang, S.; Yang, P.; Xia, J.; Wang, W.; Cai, W.; Chen, N.; Hu, S.; Luo, X.; Li, J.; Zhan, C. Land use/land cover prediction and analysis of the middle reaches of the Yangtze River under different scenarios. *Sci. Total Environ.* **2022**, *833*, 155238. [CrossRef]
29. Murakami, D.; Yoshida, T.; Yamagata, Y. Gridded GDP Projections Compatible with the Five SSPs (Shared Socioeconomic Pathways). *Front. Built Environ.* **2021**, *7*, 760306. [CrossRef]
30. Chen, Y.; Guo, F.; Wang, J.; Cai, W.; Wang, C.; Wang, K. Provincial and gridded population projection for China under shared socioeconomic pathways from 2010 to 2100. *Sci. Data* **2020**, *7*, 83. [CrossRef]
31. Peng, S.; Ding, Y.; Liu, W.; Li, Z. 1 km monthly temperature and precipitation dataset for China from 1901 to 2017. *Earth Syst. Sci. Data* **2019**, *11*, 1931–1946. [CrossRef]
32. Niu, L.; Zhang, Z.; Liang, Y.; Huang, Y. Assessing the Impact of Urbanization and Eco-Environmental Quality on Regional Carbon Storage: A Multiscale Spatio-Temporal Analysis Framework. *Remote Sens.* **2022**, *14*, 4007. [CrossRef]
33. Jin, S.; Yang, F. Carbon stock estimation and analysis of crops in Jiangxi. *Guangdong Agric. Sci.* **2011**, *38*, 216–218. [CrossRef]
34. Hu, F.; Yan, Y.; Liu, L.; Cao, Y.; Ma, Y.; Chen, M.; Liu, Z. Biomass allocation patterns in the temperate typical steppe of Inner Mongolia. *Acta Prataculturae Sinica.* **2017**, *26*, 33–42. [CrossRef]
35. Liu, Y.; Wang, T.; Gao, Y.; Dang, X.; Wang, J.; Chen, Y.; Jia, C. Characteristics and distribution pattern of carbon storage variation of the corn farmland ecosystem in the ecotone between agriculture and animal husbandry. *Agric. Res. Arid. Areas* **2015**, *33*, 214–219+229. [CrossRef]
36. Luo, H. Advances on carbon storage in crops of China. *Ecol. Environ. Sci.* **2014**, *23*, 692–697. [CrossRef]

37. Xue, J.; Hou, S.; Wu, T. A dynamic analysis of carbon emission, economic growth and industrial structure of inner mongolia based on VECM model. *J. Inn. Mong. Univ. (Nat. Sci. Ed.)* **2020**, *51*, 129–134. [CrossRef]
38. Fang, J.; Guo, Z.; Piao, S.; Chen, A. Terrestrial vegetation carbon sinks in China, 1981–2000. *Sci. China Ser. D Earth Sci.* **2007**, *50*, 1341–1350. [CrossRef]
39. Shan, Y.; Guan, D.; Liu, J.; Mi, Z.; Liu, Z.; Liu, J.; Schroeder, H.; Cai, B.; Chen, Y.; Shao, S.; et al. Methodology and applications of city level CO2 emission accounts in China. *J. Clean. Prod.* **2017**, *161*, 1215–1225. [CrossRef]
40. Shan, Y.; Guan, D.; Zheng, H.; Ou, J.; Li, Y.; Meng, J.; Mi, Z.; Liu, Z.; Zhang, Q. China CO2 emission accounts 1997–2015. *Sci. Data* **2018**, *5*, 170201. [CrossRef]
41. Sun, W.; Wu, R. Study on the balance of carboon budget and its spatial differentiation in Yangtze River Delta. *Geogr. Res.* **2012**, *31*, 2220–2228.
42. Liang, X.; Guan, Q.; Clarke, K.C.; Liu, S.; Wang, B.; Yao, Y. Understanding the drivers of sustainable land expansion using a patch-generating land use simulation (PLUS) model: A case study in Wuhan, China. *Comput. Environ. Urban Syst.* **2021**, *85*, 101569. [CrossRef]
43. Yang, X.D.; Bai, Y.P.; Che, L.; Qiao, F.W.; Xie, L.X. Incorporating ecological constraints into urban growth boundaries: A case study of ecologically fragile areas in the Upper Yellow River. *Ecol. Indic.* **2021**, *124*, 107436. [CrossRef]
44. O'Neill, B.C.; Tebaldi, C.; Van Vuuren, D.P.; Eyring, V.; Friedlingstein, P.; Hurtt, G.; Knutti, R.; Kriegler, E.; Lamarque, J.F.; Lowe, J.; et al. The Scenario Model Intercomparison Project (ScenarioMIP) for CMIP6. *Geosci. Model Dev.* **2016**, *9*, 3461–3482. [CrossRef]
45. Chuai, X.; Huang, X.; Wang, W.; Zhao, R.; Zhang, M.; Wu, C. Land use, total carbon emissions change and low carbon land management in Coastal Jiangsu, China. *J. Clean. Prod.* **2015**, *103*, 77–86. [CrossRef]
46. Li, Z.; Luan, W.; Zhang, Z.; Su, M. Relationship between urban construction land expansion and population/economic growth in Liaoning Province, China. *Land Use Policy* **2020**, *99*, 105022. [CrossRef]
47. Hastie, A.; Honorio Coronado, E.N.; Reyna, J.; Mitchard, E.T.A.; Åkesson, C.M.; Baker, T.R.; Cole, L.E.S.; Oroche, C.J.C.; Dargie, G.; Dávila, N.; et al. Risks to carbon storage from land-use change revealed by peat thickness maps of Peru. *Nat. Geosci.* **2022**, *15*, 369–374. [CrossRef]
48. Tian, S.; Wang, S.; Bai, X.; Luo, G.; Li, Q.; Yang, Y.; Hu, Z.; Li, C.; Deng, Y. Global patterns and changes of carbon emissions from land use during 1992–2015. *Environ. Sci. Ecotechnol.* **2021**, *7*, 100108. [CrossRef]
49. Fan, J.; Wang, H.; Zhou, D.; Ma, N.; Liu, B. Policy approaches to increase carbon sequestration capacity by optimizing layouts of ecological construction. *Bull. Chin. Acad. Sci.* **2022**, *37*, 459–468. [CrossRef]
50. Chen, C.; Park, T.; Wang, X.; Piao, S.; Xu, B.; Chaturvedi, R.K.; Fuchs, R.; Brovkin, V.; Ciais, P.; Fensholt, R.; et al. China and India lead in greening of the world through land-use management. *Nat. Sustain.* **2019**, *2*, 122–129. [CrossRef] [PubMed]
51. Wang, M.; Wang, Y.; Wu, Y.; Yue, X.; Wang, M.; Hu, P. Identifying the spatial heterogeneity in the effects of the construction land scale on carbon emissions: Case study of the Yangtze River Economic Belt, China. *Environ. Res.* **2022**, *212*, 113397. [CrossRef]
52. Chuai, X.; Yuan, Y.; Zhang, X.; Guo, X.; Zhang, X.; Xie, F.; Zhao, R.; Li, J. Multiangle land use-linked carbon balance examination in Nanjing City, China. *Land Use Policy* **2019**, *84*, 305–315. [CrossRef]
53. Yang, Y.; Wang, K.; Liu, D.; Zhao, X.; Fan, J. Effects of land-use conversions on the ecosystem services in the agro-pastoral ecotone of northern China. *J. Clean. Prod.* **2020**, *249*, 119360. [CrossRef]
54. Deng, L.; Liu, G.-B.; Shangguan, Z.-P. Land-use conversion and changing soil carbon stocks in China's 'Grain-for-Green' Program: A synthesis. *Glob. Chang. Biol.* **2014**, *20*, 3544–3556. [CrossRef] [PubMed]
55. Zhu, G.; Qiu, D.; Zhang, Z.; Sang, L.; Liu, Y.; Wang, L.; Zhao, K.; Ma, H.; Xu, Y.; Wan, Q. Land-use changes lead to a decrease in carbon storage in arid region, China. *Ecol. Indic.* **2021**, *127*, 107770. [CrossRef]
56. Hou, D.; Meng, F.; Prishchepov, A.V. How is urbanization shaping agricultural land-use? Unraveling the nexus between farmland abandonment and urbanization in China. *Landsc. Urban Plan.* **2021**, *214*, 104170. [CrossRef]
57. Wertebach, T.-M.; Hölzel, N.; Kämpf, I.; Yurtaev, A.; Tupitsin, S.; Kiehl, K.; Kamp, J.; Kleinebecker, T. Soil carbon sequestration due to post-Soviet cropland abandonment: Estimates from a large-scale soil organic carbon field inventory. *Glob. Chang. Biol.* **2017**, *23*, 3729–3741. [CrossRef]
58. Schierhorn, F.; Muller, D.; Beringer, T.; Prishchepov, A.V.; Kuemmerle, T.; Balmann, A. Post-Soviet cropland abandonment and carbon sequestration in European Russia, Ukraine, and Belarus. *Glob. Biogeochem. Cycles* **2013**, *27*, 1175–1185. [CrossRef]
59. Xie, H.; Zhai, Q.; Wang, W.; Yu, J.; Lu, F.; Chen, Q. Does intensive land use promote a reduction in carbon emissions? Evidence from the Chinese industrial sector. *Resour. Conserv. Recycl.* **2018**, *137*, 167–176. [CrossRef]
60. Lu, F.; Hu, H.; Sun, W.; Zhu, J.; Liu, G.; Zhou, W.; Zhang, Q.; Shi, P.; Liu, X.; Wu, X.; et al. Effects of national ecological restoration projects on carbon sequestration in China from 2001 to 2010. *Proc. Natl. Acad. Sci. USA* **2018**, *115*, 4039–4044. [CrossRef]
61. Piao, S.; Yue, C.; Ding, J.; Guo, Z. Perspectives on the role of terrestrial ecosystems in the 'carbon neutrality' strategy. *Sci. China Earth Sci.* **2022**, *65*, 1178–1186. [CrossRef]
62. Lyu, X.; Li, X.; Dang, D.; Dou, H.; Wang, K.; Lou, A. Unmanned Aerial Vehicle (UAV) Remote Sensing in Grassland Ecosystem Monitoring: A Systematic Review. *Remote Sens.* **2022**, *14*, 1096. [CrossRef]